Biomaterials 31 (2010) 1307–1315

Contents lists available at ScienceDirect

Biomaterials

journal homepage: www.elsevier.com/locate/biomaterials

Nanoparticles functionalised with recombinant single chain Fv antibody fragments (scFv) for the magnetic resonance imaging of cancer cells

Kim L. Vigor [a,1], Panagiotis G. Kyrtatos [b,1], Shane Minogue [c], Khuloud T. Al-Jamal [d], Heide Kogelberg [a], Berend Tolner [a], Kostas Kostarelos [d], Richard H. Begent [a], Quentin A. Pankhurst [e], Mark F. Lythgoe [b,2], Kerry A. Chester [a,*,2]

[a] UCL Cancer Institute, Paul O'Gorman Building, 72 Huntley Street London WC1E 6DD, UK
[b] Centre for Advanced Biomedical Imaging, Department of Medicine and Institute of Child Health, University College London, Paul O'Gorman Building, 72 Huntley Street London WC1E 6DD, UK
[c] Centre for Molecular Cell Biology, Department of Medicine, Royal Free and University College Medical School UCL, London UK
[d] Nanomedicine Lab Centre for Drug Delivery Research, The School of Pharmacy, University of London, London WC1N 1AX, UK
[e] Davy-Faraday Research Laboratories, The Royal Institution of Great Britain, 21 Albemarle Street, London W1S 4BS, UK

ARTICLE INFO

Article history:
Received 4 August 2009
Accepted 14 October 2009
Available online 4 November 2009

Keywords:
Nanoparticles
Functionalisation
Targeting
Antibody
scFv
MRI

ABSTRACT

Superparamagnetic iron oxide nanoparticles (SPIONs) can substantially improve the sensitivity of magnetic resonance imaging (MRI). We propose that SPIONs could be used to target and image cancer cells if functionalised with recombinant single chain Fv antibody fragments (scFv). We tested our hypothesis by generating antibody-functionalised (ab*f*) SPIONs using a scFv specific for carcinoembryonic antigen (CEA), an oncofoetal cell surface protein. SPIONs of different hydrodynamic diameter and surface chemistry were investigated and targeting was confirmed by ELISA, cellular iron uptake, confocal laser scanning microscopy (CLSM) and MRI. Results demonstrated that ab*f*-SPIONs bound specifically to CEA-expressing human tumour cells, generating selective image contrast on MRI. In addition, we observed that the cellular interaction of the ab*f*-SPIONs was influenced by hydrodynamic size and surface coating. The results indicate that ab*f*-SPIONs have potential for cancer-specific MRI.

1. Introduction

The high spatial resolution of magnetic resonance imaging (MRI) is ideally suited for detection of cancer [1] and assessment of response to therapy [2]. However, MRI has found limited application in tumour imaging due to a lack of sensitivity [3]. Advances in nanotechnology and in particular the use of superparamagnetic iron oxide nanoparticles (SPIONs) have the potential to address this limitation. SPIONs, due to their large magnetic moments, significantly increase MRI R_1 and R_2 relaxivities, leading to a marked reduction in T_1 and T_2 times [4], thus enabling sensitive visualisation *in vivo*. Clinical application of SPIONs as contrast agents has been demonstrated with two products: Endorem® and Resovist® [5]. These SPIONs are not tumour specific *per se* but instead provide positive contrast in tumours based on their uptake by healthy phagocytic cells in preference to cancerous cells.

We have recently used the agent Endorem® for cell labelling [6] and magnetic targeting to specific sites [7]. In this study, we aimed to achieve specificity by functionalising SPIONs with recombinant single chain Fv (scFv) antibodies. ScFvs have potential advantages over whole antibodies. First, with a molecular weight of ca. 30 kDa, scFvs are one-fifth the size of whole IgG antibodies [8] and yet they retain full antigen binding capacity. Thus, even when functionalised with scFvs, the relatively small diameter of the SPION is maintained. Second, unlike whole antibodies, scFvs do not contain the Fc constant domain and therefore are not able to trigger potentially harmful immune responses [8]. Third, scFvs are readily available in recombinant form and can be generated for clinical use in non-mammalian systems [9,10] with site-specific tags for purification and attachment.

The targeting potential of the scFv antibody functionalised SPIONs (ab*f*-SPIONs) to tumour cells was assessed using sm3E, a high affinity scFv reactive to carcinoembryonic antigen (CEA) [11,12]. Three different SPIONs were used to investigate the effect of

* Corresponding author. Tel.: +44 0 20 76790700; fax: +44 0 20 31082025.
E-mail address: k.chester@ucl.ac.uk (K.A. Chester).
[1] They are joint first authors of this manuscript.
[2] They are joint last authors of this manuscript.

0142-9612/$ – see front matter © 2009 Elsevier Ltd. All rights reserved.
doi:10.1016/j.biomaterials.2009.10.036

surface coating and size on the ab*f*-SPIONs targeting potential (Table 1). To test the influence of surface coating, we compared 50 nm ab*f*-SPIONs coated with either dextran alone or with dextran plus polyethylene glycol (PEG). To test the influence of hydrodynamic particle size, we compared 20 nm and 50 nm ab*f*-SPIONs, both coated with dextran plus PEG. The uptake of the ab*f*-SPIONs was studied using a CEA+ve colorectal cancer cell line and a CEA−ve melanoma cell line, unmodified SPIONs were used as negative controls for specific uptake.

2. Materials and methods

2.1. Superparamagnetic iron oxide nanoparticles

Details of the three SPIONs investigated are shown in Table 1, which gives information on hydrodynamic particle size, composition and coating as provided by the manufacturer. All three SPIONs were formulated as multi-domain iron crystal structures comprising of 35% (w/w) magnetite embedded in a matrix of dextran (40 kDa). According to the manufacturer description, for PEGylated SPIONs, 300 Da PEG chains were absorbed onto the dextran matrix. For simplicity, we named the SPIONs as follows: d50 (dextran coated 50 nm particles), PEGd50 (dextran and PEG coated 50 nm particles) and PEGd20 (dextran and PEG coated 20 nm particles).

2.2. Zeta potential of SPION

The electrical surface charge of the SPIONs was determined by measuring the zeta potential using a Zetasizer Nano ZS (Malvern Instruments, Malvern, UK). SPIONs were tested at a concentration range of 0.01–1 mg/ml in de-ionised water at pH 7.4. The average of three measurements was taken and results were expressed as zeta potential (mV) ± S.D.

2.3. Expression and purification of the anti-CEA scFv

Sm3E, a high affinity humanised anti-CEA scFv [11,12], was engineered with a C-terminal hexahistidine (His-tag) [10] to enable purification. The gene was cloned and expressed as soluble protein in the yeast *Pichia pastoris*. Production and purification of sm3E was achieved by fermentation, using a BioFlow 3000 Bioreactor (New Brunswick, New Jersey, USA) with a working volume of 10 l, followed by expanded bed immobilised metal affinity chromatography (IMAC) using established protocols [9,10] that are compliant with good manufacturing practice and clinical use [13]. Isolation of sm3E in its monomeric form was performed by size exclusion chromatography (SEC) using Sephadex 75 (GE-Healthcare, Amersham, Bucks, UK). Fractions were taken throughout SEC purification and those within the monomeric peak were pooled. Purity of this pool was confirmed by separating a sample under reducing conditions by SDS-PAGE on 12% Tris–Glycine gel (Invitrogen, California, USA), using SeeBlue Plus2 Pre-Stained Standard (Invitrogen) as a reference. The gel was stained for 1 h at room temperature with 0.25% w/v Coomassie brilliant blue R250 dye dissolved in 10% glacial acetic acid, 30% methanol and 60% dH_2O (buffer 1). After subsequent destaining in buffer 1 (without dye), the gel was dried using Gel-dry™ drying solution (Invitrogen). CEA immunoreactivity was confirmed by ELISA (see below; *CEA ELISA*).

2.4. Surface modification of dextran SPIONs with sm3E ScFv

Modification of the d50 SPION with sm3E was achieved by adaptation of the sodium periodate method [14]. Briefly, 1 ml of 10 mg/ml d50 was added to 1 ml 10 mM sodium periodate in 0.2 M sodium acetate buffer pH 6 (Sigma–Aldrich, St Louis, USA) and incubated at room temperature for 1 h in the dark on a rotating shaker, to allow partial oxidation of the dextran. Oxidation was terminated by application of the reaction mix to a PD-10 desalting column (GE-Healthcare) which was equilibrated and eluted with 10 mM sodium acetate buffer pH 4. Conjugation (Fig. 1A) was achieved by addition of the eluted oxidised d50 (3 ml at 3 mg/ml) to sm3E (1 ml of 0.1 mg/ml in 10 mM sodium acetate buffer pH 4) and incubation on a rotating shaker for 24 h at room temperature. Subsequently, the mixture was reduced by addition of 0.1 M sodium borohydride (0.5 ml) (Sigma–Aldrich) for 15 min at room temperature. The reaction was terminated by application to a PD-10 desalting column as described above for the oxidation reaction. The ab*f*-d50 SPION conjugate (7 ml) was concentrated to 2 ml using Vivaspin 15R concentrators (Sartorius Stedim Biotech GmbH, Goettingen, Germany) with a 5000 Da cut off at 3082 g, and purified by SEC using Sephacryl 300HR (GE-Healthcare, Amersham, Bucks, UK) in PBS buffer.

Table 1
Nomenclature and surface coatings of SPION investigated.

Name	Product	Suppplier	SPION Coating
d50	50 nm nanomag®-D-spio	Micromod Partikeltechnologie GMbH	Dextran–OH
PEGd50	50 nm nanomag®-D-spio –PEG–COOH	Micromod Partikeltechnologie GMbH	Dextran–PEG–COOH
PEGd20	20 nm nanomag®-D-spio –PEG–COOH	Micromod Partikeltechnologie GMbH	Dextran–PEG–COOH

2.5. Surface modification of carboxylated PEG SPIONs with sm3E ScFv

Functionalisation of the PEGd50 and PEGd20 SPION with sm3E was achieved using a modification of the carbodiimide method [15]. Briefly, 10 mg/ml of SPION was activated by incubation with 0.6 mg 1-ethyl-3-(3-dimethylaminopropyl)-carbodiimide hydrochloride (Sigma–Aldrich) and 1.2 mg *N*-hydroxysuccinimide (Sigma–Aldrich) in 0.2 ml of 0.5 M MES buffer pH 6.3 for 1 h at room temperature on a rotating shaker. The reaction was terminated by application to PD-10 desalting columns, which was equilibrated and eluted with 0.1 M MES buffer pH 6.3. The activated PEGd50 and PEGd20 SPION (2 ml at 4.5 mg/ml) were added to sm3E (1 ml of 0.1 mg/ml in 0.1 M MES buffer pH 6.3) and the conjugation reaction (Fig. 1B) was achieved by incubation for 24 h on a rotating shaker at room temperature. After 24 h, 0.1 ml of 25 mM glycine in PBS was added to the conjugation reaction and the mixture was incubated for a further 30 min at room temperature to block remaining reactive sites. The resulting ab*f*-PEGd50 and ab*f*-PEGd20 SPION conjugates were concentrated to 2 ml using Vivaspin 15R concentrators with a 5000 Da cut off at 3082 g and then purified by SEC on Sephacryl 300HR in PBS.

2.6. ScFv-SPION ratio

The concentration of sm3E in the purified ab*f*-SPION conjugate solutions was determined using the Bradford assay as follows: 0.5 ml of the conjugate solution was added to 0.5 ml of Bradford reagent (Sigma–Aldrich) and mixed gently by hand. Samples were then incubated at room temperature for 15 min, after which absorbance was measured at 595 nm (Cecil CE2041 2000 series spectrophotometer) blanked against non-functionalised SPIONs. The absorbance reading was used to estimate the sm3E protein concentration in the samples by reading against a standard curve of serial dilutions of sm3E. Subsequently, the number of sm3E molecules in the ab*f*-SPION conjugate solutions was calculated.

The concentration of the SPIONs in the purified abf-SPION conjugate solutions was determined by absorbance readings at 490 nm. The absorbance readings were used to estimate the SPION concentration in the samples by reading against a standard curve of serial dilutions. The number of particles per mg of SPION (inclusive of iron, dextran and PEG) was taken from the manufacturer's data sheet. This was 1.1×10^{13} for the d50 and PEGd50 and 1.6×10^{14} for the PEGd20. The number of SPIONs/ml was estimated by multiplying the SPION concentration by the number of particles/mg.

2.7. CEA ELISA

Immunoreactivity of the ab*f*-SPION conjugates to CEA was tested by ELISA. CEA (Sigma–Aldrich; 100 μl of 1 μg/ml in PBS), was coated onto 96-well plates (Costa, High Wycombe, UK) and incubated overnight at 4 °C. Control wells were coated with PBS alone. The wells were then blocked with 200 μl of 5% (w/v) powdered milk in PBS for 1 h at room temperature and washed in PBS prior to incubation with 100 μl of the purified ab*f*-SPION conjugates for 1 h (in triplicate wells). Following incubation, the wells were washed with PBS and incubated with mouse anti-His IgG (Qaigen Ltd, Crawley UK) 1 μg/ml for 1 h. The wells were then washed in PBS, incubated with sheep anti-mouse-HRP (GE-Healthcare) 1 μg/ml for 1 h, washed in PBS and incubated with 100 μl of 0.4 mg/ml O-phenylenediamine dihydrochloride (Sigma–Aldrich) dissolved in phosphate citrate buffer, pH 5.0. Reactions were stopped with 50 μl 4 M HCL and the absorbance was measured at 490 nm using an Opsys MR™ Microplate Reader (Dynex Technologies, Virginia, USA).

2.8. Cell culture

LS174T, a CEA-expressing (CEA+ve) adherent colorectal cancer cell line and A375M, a CEA negative (CEA−ve) adherent melanoma cell line were obtained from the Health Protection Agency Culture Collection. The cell lines were routinely cultured at 37 °C in a humidified atmosphere with 5% CO_2 in vented 75 cm^2 flasks containing 15 ml RPMI-1640 medium supplemented with 10% foetal calf serum (FCS), 2 mM L-glutamine, 50 IU/ml penicillin, 50 μg/ml streptomycin and 5% non-essential amino acids (PAA Laboratories GmbH, Pasching, Austria). For subculture, the cells were split at a ratio of 1:5 when 80% confluence was reached. The cells were washed with PBS followed by incubated with trypsin–EDTA solution (PAA Laboratories) for 10 min at 37 °C to detach the cells. Once detached the cells were resuspended in complete media at room temperature, washed twice by centrifugation, resuspended in complete media and reseeded into new culture flasks.

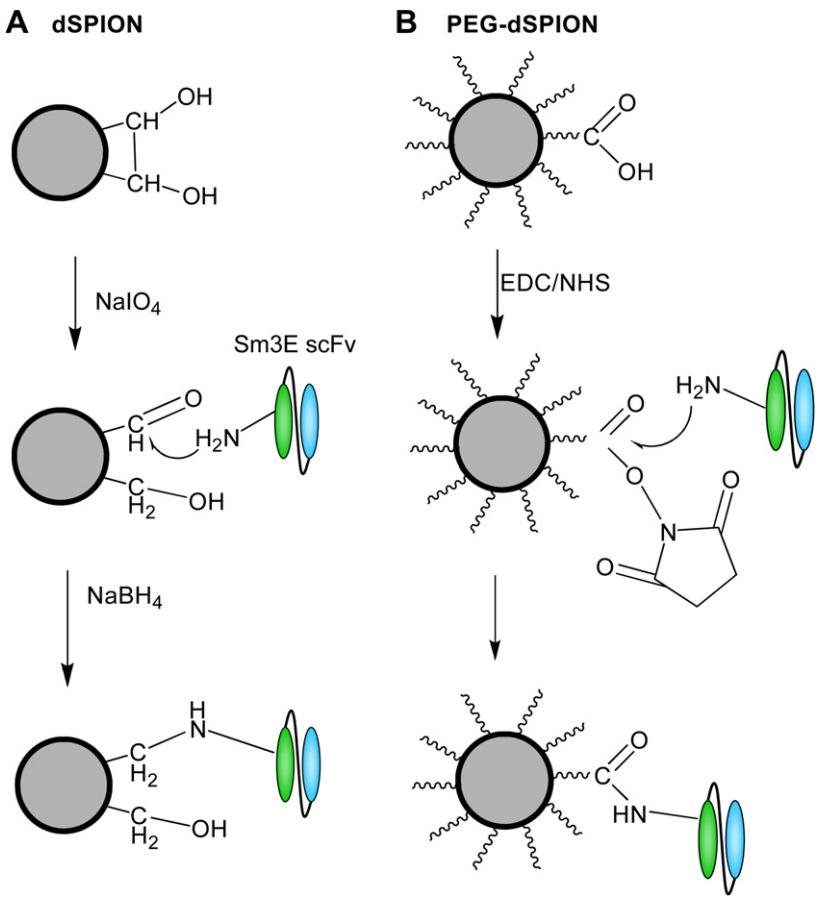

Fig. 1. ab*f*-SPION conjugation schemes. A) Functionalisation of d50 SPIONs with sm3E. (B) Functionalisation of PEGd50 SPIONs with sm3E.

2.9. Cellular uptake and trafficking studies by confocal laser scanning microscopy (CLSM)

The specificity and cellular uptake pattern of the sm3E functionalised SPIONs to CEA+ve or CEA−ve cells was examined by CLSM. Cells were grown as a monolayer on circular coverslips (VWR) in 24 well plates at a density of 1×10^5 cells/ml, 500 μl/coverslip. The cells were incubated overnight at 37 °C in a humidified incubator with a CO_2 concentration of 5%, to allow adherence of the cells. The cells were then incubated a further 24 h with 0.5 ml culture media containing i) media alone, ii) non-functionalised SPIONs at 0.1 mgSPION/ml, or iii) ab*f*-SPIONs at 0.1 mgSPION/ml. Following incubation, cell monolayers were washed three times in PBS, fixed in 4% paraformaldehyde for 20 min on ice. Once fixed the cells were washed in PBS to remove the paraformaldehyde and incubated with mouse anti-dextran IgG (Stemcell Technologies Inc, Vancouver, Canada) for 45 min at room temperature. The cells were again washed in PBS and further incubated with goat anti-mouse IgG1 antibody labelled with Alexa Fluor 564 (Invitrogen, Oregon, USA). Nuclei were counterstained using Hoechst 33342 (Invitrogen) according to the manufacturer's instructions. Endosomal localisation of SPIONs was investigated by co-immunstaining with an anti-LAMP1 monoclonal antibody directed against late endosomal/lysosome. Fluorescent labelling of the endosomes as well as the SPIONs allowed CLSM analysis of SPION-endosome co-localisation. For fluorescent labelling of both the endosomes and SPIONs, the cells were co-incubated with mouse anti- LAMP1 IgG2b (BD Bioscience, New Jersey, USA) and mouse anti-dextran IgG1 μg/ml, followed by co-incubation with goat anti-mouse IgG2b labelled with Alexa Fluor 488 and goat anti-mouse IgG1 labelled with Alexa Fluor 564. Nuclei were counterstained using Hoechst 33342. Coverslips were mounted in ProLong antifade (Invitrogen) and imaged by using a Zeiss LSM 510 meta confocal microscope. All antibodies in this experiment were used at 1 μg/ml.

2.10. Cellular SPION uptake studies by ferrozine assay

Cellular uptake of the ab*f*-SPIONs was quantified using an adaptation of the ferrozine assay [16]. The CEA+ve cells were seeded at a density of 1×10^5 cells/ml per well in 24 well plates. Once confluent and no further growth observed (typically after 5 days) the cells were incubated for a further 24 h with 1 ml of fresh culture medium containing i) media alone, ii) non-functionalised SPIONs at 0.1 mgSPION/ml or iii) ab*f*-SPIONs at 0.1 mgSPION/ml. Following incubation, the cells were washed in ice cold PBS. After completely removing the PBS, the cells in three of the media control wells were trypsonised and counted to determine the average number of cells per well. All other treated and control cells were lysed with 0.3 ml of 50 mM NaOH (Sigma–Aldrich) for 2 h at room temperature. The cell lysates were then transferred to 1 ml Eppendorf tubes (Eppendorf North America, New York, USA) and mixed gently by hand with 0.3 ml of 10 mM HCl (Sigma–Aldrich) and 0.3 ml of the iron releasing reagent, a freshly mixed solution of equal volumes of 1.4 M HCl and 4.5% (w/v) $KMnO_4$ (Sigma–Aldrich). The reaction mix was incubated for 2 h at 60 °C and cooled to room temperature before addition of 30 μl of the iron detection reagent (6.5 mM ferrozine, 6.5 mM neocuproine, 2.5 M ammonium acetate and 1 M ascorbic acid [Sigma–Aldrich] in water). After gentle mixing by hand, the samples were incubated at room temperature for a further 30 min to allow colour development. Absorbance was measured at 550 nm. The absorbance values were used to estimate the SPION iron concentration in the samples by reading against a standard curve of serial dilutions of the d50, PEGd50 or PEGd20 SPION. The absorbance values were used to estimate the SPION iron concentration in the samples by reading against a standard curve of serial dilutions of the d50, PEGd50 or PEGd20 SPION; individual cell uptake of SPIONs was estimated by dividing the number of cells/well.

2.11. In vitro cytotoxicity

SPION cytotoxicity was investigated using the 3-(4,5-Dimethylthiazol-2-yl)-2,5-diphenyltetrazolium bromide (MTT) assay (Sigma–Aldrich) [17]. CEA +ve cells were seeded at a density of 1×10^5 cells/ml, 200 μl/well in 96-well plates. The plates were incubated overnight in a humidified incubator with a CO_2 concentration of 5% to allow adherence of the cells. Once adhered the cells were incubated overnight with either 0.1 ml of medium containing no SPIONs, the unmodified SPION at particle concentrations of 0.1 mg/ml, 0.5 mg/ml or 1 mg/ml or the ab*f*-SPION at a particle concentration of 0.1 mg/ml. The cells were then washed and incubated a further 96 h in fresh culture media. 20 μl (5 mg/ml) MTT was added and incubation was continued for a further 4 h. The medium was carefully removed and the formazan crystals (indicating cell viability) were solubilised by adding 0.1 ml dimethyl sulfoxide (Sigma–Aldrich) per well. Absorbance at 550 nm was measured using the Opsys MR™ Microplate Reader (Dynex Technologies). Experiments were performed in triplicate and are expressed as the average +/− S.D. Cell survival was determined

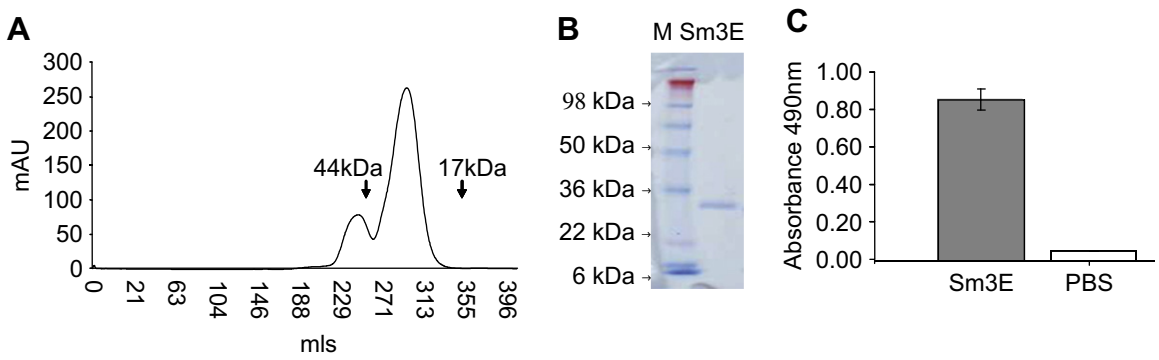

Fig. 2. Purification of sm3E expressed in *P.pastoris*. A) SEC profile of purified sm3E. The 1st peak is dimeric sm3E, eluted between 230 ml and 270 ml. The second larger peak corresponds to the monomeric sm3E, eluted between 270 ml and 340 ml. Molecular weight (MW) standards are shown. B) Coomassie-stained SDS-PAGE gel containing pooled monomeric fractions of sm3E from SEC purification, demonstrating purity of the scFv. M is the protein MW marker. C) CEA ELISA showing immunoreactivity of the purified sm3E to CEA.

as a percentage of viable cells in comparison with media only control wells. One-way ANOVA and unpaired t-tests were used to determine whether the SPIONs caused any significant cytotoxicity.

2.12. Magnetic resonance imaging

The potential of ab*f*-SPION conjugates for MRI was investigated *in vitro* after incubation in the CEA+ve or CEA−ve cells. Cells cultured to 70% confluency in a T75 flask were incubated overnight in 10 ml of fresh culture medium containing i) media alone, ii) non-functionalised SPIONs at 0.1 mgSPION/ml, or iii) ab*f*-SPION at 0.1 mgSPION/ml. After incubation, the cells were washed before and after trypsinisation in PBS and fixed in 4% paraformaldehyde for 20 min. Following fixation, the cells were washed again in PBS and pelleted by centrifugation in 0.25 ml Eppendorf tubes. Supernatants were removed and the tubes were placed inside a modified 50 ml test tube filled with 16 mM $CuSO_4$ to enhance image contrast. T_2-weighted images were acquired with a 2DFT spin-echo sequence on a 2.35T horizontal bore scanner interfaced to a SMIS console (3 cm RF coil, 256 × 256 matrix, 1 mm slice, 2 averages, FOV 60 mm, TR = 1 s, TE = 80 ms). T_2 relaxation times were obtained from 12 echo times (TE = 28–80 ms, 128 × 128 matrix, FOV 40 mm, TR = 1 s) and calculated for each sample on a pixel-by-pixel basis.

3. Results

3.1. Functionalisation of SPIONs

A total of 150 mg of monomeric sm3E was generated from a 10 l fermentation after purification by EBA-IMAC followed by SEC (Fig. 2A). The material obtained gave a single band of ca. 27 kDa in SDS-PAGE that is in agreement with the molecular mass as deduced from the sm3E-His amino acid sequence (Fig. 2B). Immunoreactivity with CEA was confirmed by ELISA (Fig. 2C).

The purified sm3E was covalently conjugated to d50 SPIONs via dextran and to the PEGylated SPIONs via carboxylated PEG. Attachment and purification by size exclusion chromatography was successful in all cases and resulted in an estimated 28 sm3E molecules per SPION for the ab*f*-d50 and 29 for ab*f*-PEGd50. For the smaller ab*f*-PEGd20 SPION the estimated number of scFvs was only 2 sm3E molecules per particle. This was directly proportional to the PEG content of the SPION as stated on the manufacturers data sheet, which gave an estimation of 131 PEG chains per PEGd20 compared to 1900 PEG chains per PEGd50. All the functionalised SPIONs bound specifically to the target antigen, CEA, as shown by ELISA (Fig. 3) CEA binding was not detected with unmodified SPIONs (Fig. 3).

3.2. In vitro cytotoxicity

Potential cytotoxicity of the ab*f*-SPIONs and the non-functionalised SPIONs was estimated from cell viability relative to untreated cells. There was 92–100% cell viability in relation to the control sample (Fig. 4). These results indicate that there is no evidence of SPION toxicity at concentrations up to 1 mg/ml.

3.3. Targeting and imaging

The ability of the ab*f*-SPIONs to specifically target and image CEA-expressing cells was tested using complementary imaging techniques. CLSM was used to visualise cellular distribution of SPIONs and MRI was used to quantify the T_2 of cell samples and assess the imaging potential of the conjugates. In all cases, CEA+ve or CEA−ve cells were pre-incubated with ab*f*-SPIONs or unmodified SPIONs at a particle concentration of 0.1 mg/ml. This was equivalent to 1.3 μg scFv/ml for 50 nm particles and to 1.5 μg scFv/ml for 20 nm particles. The results displayed in Fig. 5 demonstrate that functionalisation with scFvs was an essential requirement for specific binding to CEA+ve cells, for all particles tested. However, the different coatings and hydrodynamic radii gave rise to distinct cellular interaction properties.

3.4. Dextran coated SPIONs

The dextran coated ab*f*-d50 SPIONs specifically targeted the CEA+ve cells and showed preferential distribution around the cell surface membrane (Fig. 5A, CLSM, CEA+ve cells, ab*f*-d50). In

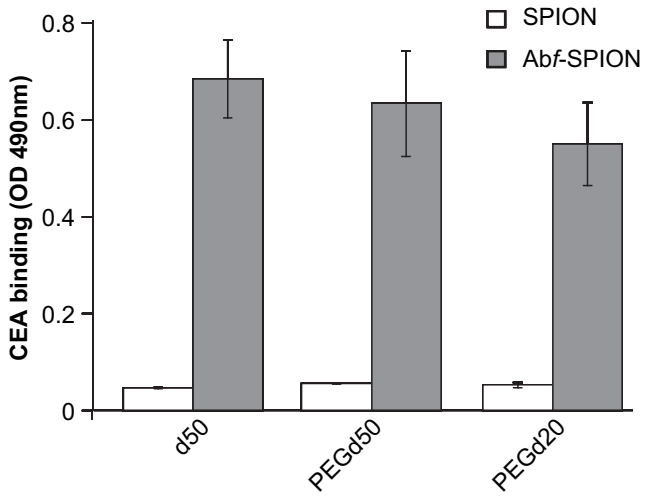

Fig. 3. CEA ELISA confirming immunoreactivity of the ab*f*-d50, ab*f*-PEGd50 and ab*f*-PEGd20 to CEA. The non-functionalised d50, PEGd50 and PEGd20 did not exhibit binding to CEA.

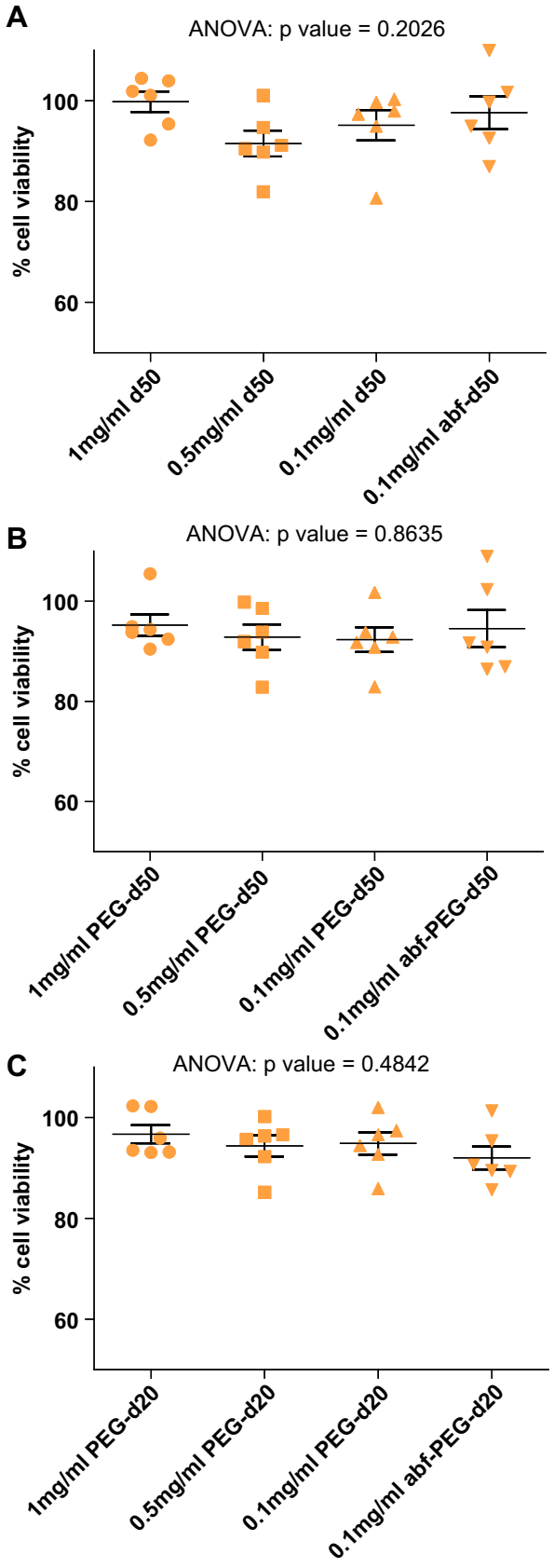

Fig. 4. Cell viability after overnight incubation with functionalised and non-functionalised A) d50, B) PEGd50 and C) PEGd20. From one-way ANOVA and unpaired t-tests (not shown) no significant difference in cell viability was observed against the media only control.

contrast, the non-functionalised d50 particles showed no binding (Fig. 5 A, CLSM, CEA+ve cells, d50). The specificity for CEA was confirmed by the cellular uptake of iron which, using the Ferrozine assay, was estimated to be 4.4 pgSPION/cell for cells targeted with ab*f*-d50 and <0.01 pgSPION/cell with unmodified d50. On visual inspection of CLSM images neither ab*f*-d50 nor unmodified d50 bound significantly to the CEA−ve cells (Fig. 5A, CLSM, CEA−ve cells). Specificity of the ab*f*-SPIONs was further supported by *in vitro* MRI. T_2-weighted images of CEA+ve cells incubated with ab*f*-d50 demonstrated a negative T_2 contrast (Fig. 5A, MRI, CEA+ve cells) as a result of a T_2 reduction of 43% compared to media only control (Fig. 5A, T_2 Chart, CEA+ve cells). A very small reduction in T_2 (0.17%) was observed with the non-functionalised d50. Following incubation with CEA−ve cells, a reduction in T_2 was also obtained with both the functionalised and non-functionalised d50 (28% and 20% respectively, Fig. 5A, T_2 Chart, CEA−ve cells). However, no resulting contrast was observed on T_2-weighted MR images (Fig. 5A, MRI, CEA−ve cells).

3.5. PEGylated SPION

Addition of PEG–COOH to the SPION surface promoted internalisation of the 50 nm particles and tended to encourage non-specific uptake as shown in Fig. 5B. Here, internalisation was observed both for sm3E-conjugated particles (Fig. 5B, CLSM, CEA+ve cells, ab*f*-PEGd50) and unmodified particles (Fig. 5B, CLSM, CEA+ve cells, PEGd50). The internalised particles appeared to be trafficked to endosomes (see relevant section below). However, functionalisation with sm3E led to a CEA-specific increase in uptake. The estimated cellular iron content using ab*f*-PEGd50 was 4.7 pgSPION/cell. For PEGd50, this was <0.01 pgSPION/cell. These results are similar to those obtained with the non-PEGylated d50 particles. A similar trend was observed on T_2-weighted MR images (Fig. 5B, MRI). CEA+ve cells incubated with ab*f*-PEGd50 exhibited a 57% reduction in T_2, compared to 11% reduction with unmodified PEGd50 (Fig. 5B, T_2 Chart, CEA+ve cells).

The PEGd50 showed significant intracellular uptake in CEA−ve cells; this was independent of functionalisation (Fig. 5B, CLSM, CEA−ve cells). In support of these observations, MR images showed negative contrast and there was a corresponding reduction in T_2 using both the functionalised and the non-functionalised PEGd50 on CEA−ve cells (51% and 49% reduction in T_2, respectively) (Fig. 5B, MRI and T_2 Chart, CEA−ve cells). Together, these results indicate the non-specific interaction of the PEGd50 with the CEA−ve cells.

When PEGylated particles with a smaller hydrodynamic radius were tested, specific internalisation was still retained but non-specific uptake was decreased. This is illustrated in Fig. 5C, where internalisation of ab*f*-PEGd20 is demonstrated, whereas uptake is decreased in the absence of functionalisation with sm3E (Fig. 5C, CLSM, CEA+ve cells). This was mirrored by the difference in CEA+ve cellular iron content between the particles, which was 2.4 pgSPION/cell for ab*f*-PEGd20 and <0.01 pgSPION/cell for unmodified PEGd20. The iron uptake with ab*f*-PEGd20 was approximately half that achieved with the larger ab*f*-PEGd50 and may reflect the fact that we were able to attach >10-fold less sm3E to the smaller particles. Importantly, however, even with reduced iron uptake, the ab*f*-PEGd20 provided specific MR contrast on CEA+ve cells (Fig. 5C, MRI, CEA+ ve cells). Furthermore, the reduction in T_2 values obtained with ab*f*-PEGd20 was 51%, only marginally lower than the 57% obtained with the ab*f*-PEGd50.

Comparing favourably to the larger PEGylated particles, CLSM images illustrated minimal internalisation of the PEGd20 into CEA−ve cells, either before or after conjugation to sm3E (Fig. 5C, CLSM, CEA−ve cells). In addition, neither ab*f*-PEGd20 nor PEGd20 provided strong negative contrast on MRI using CEA−ve cells

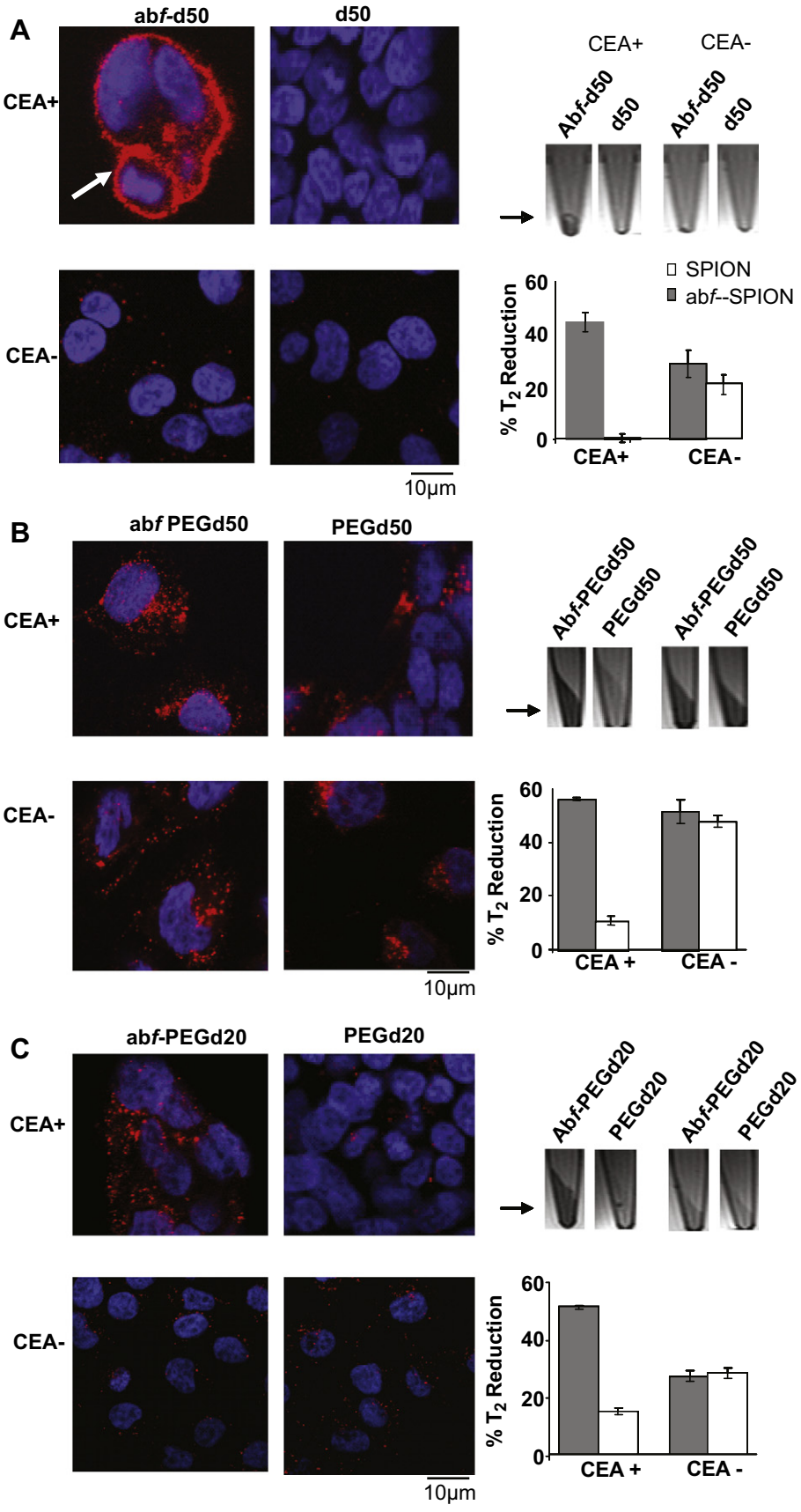

Fig. 5. CLSM and T_2-weighted images of CEA+ve LS174T cells and CEA−ve A375M cells following overnight incubation with functionalised and non-functionalised SPIONs (A) d50, (B) PEGd50 and (C) PEGd20. For the CLSM images (left panel), SPIONs are shown in red and cell nuclei in blue. Specific uptake on MRI (right panel) was illustrated by T_2-weighted spin-echo images of cell pellets in test tubes and their corresponding T_2 relaxometry values. The percentage (%) T_2 reduction values were calculated based on values from cells incubated in media alone. CLSM and T_2-weighted images indicate that ab*f*-d50 (A) bind specifically to the cell membrane of the CEA+ve cells (CLSM) causing enhanced MRI contrast of the CEA+ve cell pellet (T_2 image; arrow). In contrast, the PEGd50 (B) internalised non-specifically into both cells lines as shown by CLSM resulting in a similar MRI signal for the CEA+ve and CEA−ve cells (T_2 image; arrow). The ab*f*-PEGd20 (C) appeared to be specifically internalised into CEA+ve cells (CLSM) leading to corresponding specific enhanced MRI contrast of the cell pellet (T_2 image; arrow).

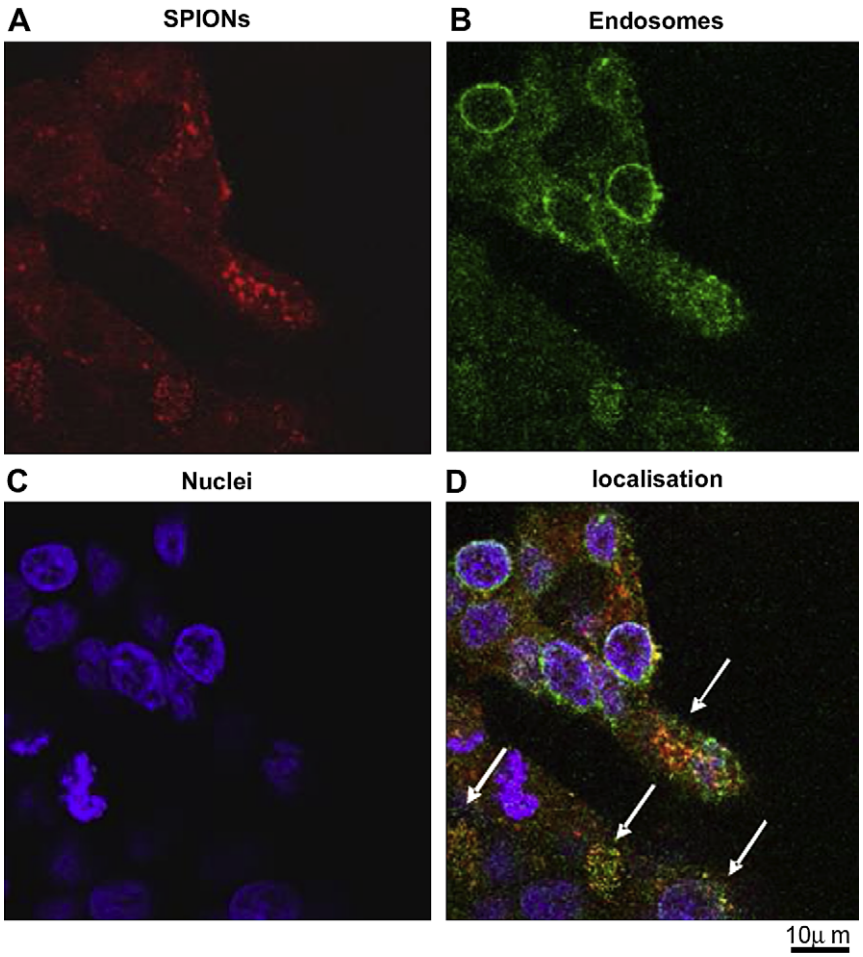

Fig. 6. CLSM images showing endosomal localisation of ab*f*-PEG-d50 in CEA+ve LS174T cells (white arrow in (D). ab*f*-PEG-d50 are shown in red (A), endosomes in green (B) and cell nuclei in blue (C).

(Fig. 5 C, MRI, CEA−ve cells). The reduction in T_2 was approximately 25% for both ab*f*-PEGd20 and PEGd20 (Fig. 5C, T_2 Chart, CEA−ve cells), which is similar to the 25% reduction obtained using the d50 particles.

3.6. Intracellular trafficking

On CLSM images the internalised PEGylated SPIONs appeared to localise to punctate structures distributed throughout the cytoplasm (Fig. 5A, CLSM, CEA+ve cells). To determine whether these represent endosomal compartments we co-immunostained the cells with anti-dextran (Fig. 6A, red) and anti-LAMP1 (Fig. 6B, green) antibodies. Co-localisation was observed between the antibodies (Fig. 6D, white arrows) indicating that the 50 nm PEGd50 are trafficked to late endosomal compartments. Similar results were obtained using the ab*f*-PEGd20 (not shown).

3.7. Surface charge

Negative surface charge has been reported to encourage non-specific electrostatic interaction with membranes and facilitate intracellular uptake [18,19]. Since the PEGylated SPIONs were coated with carboxylated PEG, we tested whether this affected the overall surface charge, and could therefore be responsible for the internalisation and the non-specificity observed with the PEGylated particles. We found that, whilst the d50 SPION had a zeta potential (surface charge) of −1.5 mV, the PEGd20 and PEGd50 have a surface charge of −4.0 mV and −5.0 mV, respectively. The intracellular uptake observed with the PEGd20 and PEGd50 may therefore be due to increased negative surface charge, attributed by the absorbed PEG–COOH chains.

4. Discussion

We have investigated the potential of scFvs to target SPIONs to cancer cells. We propose that these SPIONs could play a key role in tumour delivery of therapeutics and non-invasive monitoring of therapeutic response. In this study, we have tested the targeting potential of scFv-functionalised SPIONs by measuring their specificity and pattern of uptake in cancer cells and their MRI conspicuity *in vitro* following targeting to cancer cells. To achieve this targeting we conjugated the SPIONs to sm3E, a recombinant scFv reactive with CEA, a cell surface glycoprotein. CEA is an established tumour marker, over-expressed in many human cancers, particularly of the gastrointestinal tract [20], and a potential target for ab*f*-SPIONs. However, this approach is applicable to other cancers and indications since scFvs are readily obtained to virtually any target using phage display libraries and recombinant antibody technology [21].

We have tested SPIONs with different surface coatings and hydrodynamic ratios, identifying properties important for specific targeting to target CEA+ve cancer cells. For our initial experiments,

we focused on SPIONs stabilised with dextran, the most common particle coating for biomedical applications [22,23]. Dextran stabilises the iron oxide particles, minimising agglomeration, and also provides a platform for functionalisation [24]. It is used in the FDA-approved SPIONs Resovist™ and Endorem®. For *in vivo* applications, the size of the SPION is a critical factor in its ability to reach the tumour [25]. It is reported that SPIONs with hydrodynamic diameter over 100 nm are readily cleared by the reticuloendothelial system [26] or are unable to move through capillary vessels [27]. We therefore investigated dextran coated SPIONs in the size range of 50 nm. The molecular diameter of a whole IgG is approximately 28 nm [28], and scFvs are relatively small at approximately 5 nm. Therefore, functionalisation of SPIONs with scFvs should not significantly increase their diameter.

We observed that by attaching the scFv it was possible to achieve specific binding of the SPIONs to the CEA-expressing cells and that we could measure this using MRI, CLSM and iron uptake assays. The targeted SPIONs were localised on the extracellular membrane, as has been reported with dextran coated SPIONs functionalised with whole monoclonal antibodies (mAbs) [29]. The dextran coated SPIONs were also easy to manipulate and could be used as simple biological reagents in standard applications such as FPLC and ELISA. Whilst specificity of SPIONs may be achieved through conjugation with mAbs [25,27,29–31], mAbs can substantially increase the hydrodynamic radius when conjugated to SPIONs and may also initiate unwanted interactions with natural effectors [30].

Dextran coated particles, however, may have limited application for tumour targeting *in vivo*, due to receptor-mediated endocytosis via macrophage receptors [32]. One-way of addressing this is to mask the particles with PEG. The PEG brush-like structure results in formation of a watery shell around the particle and is thought to sterically prevent attachment of plasma proteins [33]. As a result, PEG has been shown to reduce recognition and clearance of nanoparticles [34], increasing blood circulation time from seconds to hours [35–38]. The increase in blood half-life is predicted to enable more scFv-targeted SPIONs to reach the target site. PEG has also been used in FDA-approved biotherapeutics [39].

Our comparison of PEGylated SPIONs targeting potential with dextran coated SPIONs of the same size revealed marked differences in the SPION properties, conferred by their different surfaces. Although the functionalisation with scFv still resulted in increased iron uptake, the 50 nm PEGylated SPIONs were non-specifically taken up by CEA+ve cells, even before conjugation to sm3E. Moreover, the PEGylated SPIONs showed intracellular uptake into endosomes, whereas the dextran coated particles appeared to remain on the cell surface. It has been reported that anionic SPIONs have a higher affinity for positively charged areas on the cell membrane, encouraging non-specific internalisation by fluid phase endocytosis [19]. Therefore, one possible cause of the observed internalisation would be the negative surface charge conferred by the carboxylated PEG chain terminals. Indeed, our results showed a reproducible decrease from −1 mV to −5 mV upon addition of PEG, suggesting that this is a likely contributing factor. In line with these observations, dextran has previously been reported to exhibit poor internalisation [19], an effect attributed to its neutral charge [40–43].

The quantity of PEG-mediated non-specific uptake was, however, less than 0.01 pg/cell compared to that achieved by functionalisation with scFv (4.8 pg/cell). Targeting specificity to the CEA+ve cells was also confirmed with MRI; the ab*f*-PEGd50 resulted in a marked 57% reduction in T_2 values, whereas the unmodified PEGd50 resulted in an 11% reduction in T_2, indicating a limited amount of non-specific interaction with CEA+ve cells. However, there was a 50% reduction in T_2 values for the CEA−ve cells, even in the absence of sm3E, which strongly suggests non-specific uptake by this cell line.

These results indicate that non-specific SPION uptake is not only dependent on surface charge but also on cell type. Similar findings have been reported by a number of other groups [35,40,44,45] and it has been speculated to be due to cell lines exhibiting different rates and mechanisms of endocytosis [40,45]. The architecture and composition of cells has also been found to affect SPION uptake, and PEGylated SPION have been reported to be show more non-specific cellular uptake [35]. Our results are consistent with these observations as the more PEGylated PEGd50 showed increased non-specific binding to the CEA−ve A375M cells in comparison with the non-PEGylated d50.

The intracellular uptake of SPIONs by non-specific endocytosis has also been reported to be dependent on hydrodynamic SPION size, with increasing diameter leading to increased cell uptake [38]. We hypothesised that using a smaller less PEGylated particle would reduce non-specific uptake and thus chose to investigate the potential of PEGylated 20 nm particles. Conjugation of the sm3E to the PEGd20 yielded approximately 2 scFvs per SPION. This is consistent with DeNardo et al., who reported conjugation of 2 ChL6 mAbs to the PEGd20 by carbodiimide conjugation chemistry [15]. Specific binding of the ab*f*-PEGd20 to the CEA+ve cells was observed, with SPION uptake of 2.5 pg/cell. This SPION uptake compares well to Funovic et al., who demonstrated uptake of approximately 2 pg/cell of anti-HER2 targeted SPIONs and anti-9.2.27 targeted SPIONs [27]. The sm3E-PEGd20 was readily visible on MRI when targeted to the CEA+ve cells (with a 51% reduction in T_2). This was not the case for either the non-targeted particles or the CEA−ve cells, indicating its specificity to the CEA+ve LS174T cells.

Once internalised, the PEGylated SPIONs demonstrated accumulation into endosomal compartments within the cell, a finding that agrees with previous reports [19,42,43]. Due to the conditions within these compartments, SPIONs are eventually broken down and incorporated into the plasma iron pool [46]. However, this degradation is believed to occur after several days [47], giving sufficient time for MR imaging.

5. Conclusions

We have demonstrated the functionality of three different SPIONs with the anti-CEA sm3E scFv and shown their potential as selective imaging contrast agents. Size and charge of the SPIONs were found to be important factors in the cellular behaviour of the SPIONs. The ab*f*-d50 was shown to bind selectively to the cell membrane compared to the ab*f*-PEGd50, which showed intracellular uptake and some non-specificity in particular with the CEA−ve A375M cell line. Both of these effects are believed to be attributed to the size, PEG content and anionic charge of the PEGd50. By conjugation of sm3E to the smaller, less PEGylated PEGd20, intracellular trafficking into cells was retained whilst the issue of non-specificity was reduced. Thus, the 20 nm ab*f*-PEG SPIONs appear to show superior target-dependent specificity, although a higher number of scFvs were covalently bound to the larger 50 nm ab*f*-PEG SPIONs. Our results demonstrate that, through functionalisation with scFvs, specific targeting of both dextran and PEG coated SPIONs to cells is achievable *in vitro*, while the size and surface properties of the SPIONs are important parameters to consider for optimal design. ScFv-SPION conjugates are attractive for the future development of specific vehicles aimed at cancer diagnosis and therapy.

Acknowledgements

Kim Vigor was supported by RAFT (Restoration of Appearance and Function Trust). The Authors would also like to thank Cancer Research UK, the UCL Cancer Institute Research Trust, the Rosetrees

Trust, the UCL Experimental Cancer Medicine Centre, the UCL/UCLH Comprehensive Biomedical Research Centre of the NIHR, the UCL Institute of Child Health Research Appeal Trust ,EPSRC (Engineering and Physical Sciences Research Council) Nanotechnology Grand Challenge Grant, Kings College London and UCL Comprehensive Cancer Imaging Centre CR-UK and EPSRC in association with MRC and DoH (England) and the Alexander S. Onassis Public Benefit Foundation for financial support. We are grateful to Dr Allan Hackshaw for assistance with statistical analysis and Dr Cordula Gruettner (Micromod Partikeltechnologie GMbH) and Dr Alan Green for helpful discussions.

Appendix

Figures with essential color discrimination.Many of the figures in this article have parts that are difficult to interpret in black and white. The full color images can be found in the on-line version, at doi:10.1016/j.biomaterials.2009.10.036.

References

[1] Brindle K. New approaches for imaging tumour responses to treatment. Nat Rev Cancer 2008;8:94–107.
[2] Han Z, Fu A, Wang H, Diaz R, Geng L, Onishko H, et al. Noninvasive assessment of cancer response to therapy. Nat Med 2008;14:343–9.
[3] Lee JH, Huh YM, Jun YW, Seo JW, Jang JT, Song HT, et al. Artificially engineered magnetic nanoparticles for ultra-sensitive molecular imaging. Nat Med 2007 Jan;13:95–9.
[4] Renshaw PF, Owen CS, McLaughlin AC, Frey TG, Leigh Jr JS. Ferromagnetic contrast agents: a new approach. Magn Reson Med 1986;3:217–25.
[5] Wang YX, Hussain SM, Krestin GP. Superparamagnetic iron oxide contrast agents: physicochemical characteristics and applications in MR imaging. Eur Radiol 2001;11:2319–31.
[6] Panizzo RA, Kyrtatos PG, Price AN, Gadian DG, Ferretti P, Lythgoe MF. In vivo magnetic resonance imaging of endogenous neuroblasts labelled with a ferumoxide-polycation complex. Neuroimage 2009;44:1239–46.
[7] Kyrtatos PG, Lehtolainen PL, Junemann-Ramirez M, Garcia-Prieto A, Price AN, Martin JF, et al. Magnetic tagging increases delivery of circulating progenitors in vascular injury. JACC Cardiovasc Interv 2009;2:794–802.
[8] Holliger P, Hudson PJ. Engineered antibody fragments and the rise of single-domains. Nat Biotechnol 2005;23:1126–36.
[9] Tolner B, Smith L, Begent RH, Chester KA. Production of recombinant protein in *Pichia pastoris* by fermentation. Nat Protoc 2006;1:1006–21.
[10] Tolner B, Smith L, Begent RH, Chester KA. Expanded-bed adsorption immobilized-metal affinity chromatography. Nat Protoc 2006;1:1213–22.
[11] Boehm MK, Corper AL, Wan T, Sohi MK, Sutton BJ, Thornton JD, et al. Crystal structure of the anti-(carcinoembryonic antigen) single-chain Fv antibody MFE-23 and a model for antigen binding based on intermolecular contacts. Biochem J 2000;346(Pt 2):519–28.
[12] Graff CP, Chester K, Begent R, Wittrup KD. Directed evolution of an anti-carcinoembryonic antigen scFv with a 4-day monovalent dissociation half-time at 37 degrees C. Protein Eng Des Sel 2004;17:293–304.
[13] Tolner B, Smith L, Hillyer T, Bhatia J, Beckett P, Robson L, et al. From laboratory to Phase I/II cancer trials with recombinant biotherapeutics. EurJ Cancer 2007;43:2515–22.
[14] Molday RS, MacKenzie D. Immunospecific ferromagnetic iron-dextran reagents for the labeling and magnetic separation of cells. J Immunol Methods 1982;52:353–67.
[15] DeNardo SJ, DeNardo GL, Miers LA, Natarajan A, Foreman AR, Gruettner C, et al. Development of tumor targeting bioprobes ((111)In-chimeric L6 monoclonal antibody nanoparticles) for alternating magnetic field cancer the rapy. Clin Cancer Res 2005;11:7087s–92s.
[16] Riemer J, Hoepken HH, Czerwinska H, Robinson SR, Dringen R. Colorimetric ferrozine-based assay for the quantitation of iron in cultured cells. Anal Biochem 2004;331:370–5.
[17] Mosmann T. Rapid colorimetric assay for cellular growth and survival: application to proliferation and cytotoxicity assays. J Immunol Methods 1983;65:55–63.
[18] Patil S, Sandberg A, Heckert E, Self W, Seal S. Protein adsorption and cellular uptake of cerium oxide nanoparticles as a function of zeta potential. Biomaterials 2007;28:4600–7.
[19] Wilhelm C, Billotey C, Roger J, Pons JN, Bacri JC, Gazeau F. Intracellular uptake of anionic superparamagnetic nanoparticles as a function of their surface coating. Biomaterials 2003;24:1001–11.
[20] Hammarstrom S. The carcinoembryonic antigen (CEA) family: structures, suggested functions and expression in normal and malignant tissues. Semin Cancer Biol 1999;9:67–81.
[21] Hoogenboom HR. Selecting and screening recombinant antibody libraries. Nat Biotechnol 2005;23:1105–16.
[22] Berry CC, Wells S, Charles S, Aitchison G, Curtis AS. Cell response to dextran-derivatised iron oxide nanoparticles post intern alisation. Biomaterials 2004;25:5405–13.
[23] McCarthy JR, Weissleder R. Multifunctional magnetic nanoparticles for targeted imaging and therapy. Adv Drug Deliv Rev 2008;60:1241–51.
[24] Bulte JW, Kraitchman DL. Iron oxide MR contrast agents for molecular and cellu lar imaging. NMR Biomed 2004;17:484–99.
[25] Artemov D, Mori N, Ravi R, Bhujwalla ZM. Magnetic resonance molecular imaging of the HER-2/neu receptor. Cancer Res 2003;63:2723–7.
[26] Gupta AK, Gupta M. Cytotoxicity suppression and cellular uptake enhancement of surface modified magnetic nanoparticles. Biomaterials 2005;26:1565–73.
[27] Suwa T, Ozawa S, Ueda M, Ando N, Kitajima M. Magnetic resonance imaging of esophageal squamous cell carcinoma using magnetite particles coated with anti-epidermal growth factor receptor antibody. Int J Cancer 1998;75:626–34.
[28] Roberts CJ, Williams PM, Davies J, Dawkes AC, Sefton J, Edwards JC, et al. Real-space differentiation of IgG and IgM antibodies deposited on microtitre wells by scanning force microscopy. Langmuir 1995;11:1822–6.
[29] Funovics MA, Kapeller B, Hoeller C, Su HS, Kunstfeld R, Puig S, et al. MR imaging of the her2/neu and 9.2.27 tumor antigens using immunospecific contrast agents. Magn Reson Imaging 2004;22:843–50.
[30] Suzuki M, Honda H, Kobayashi T, Wakabayashi T, Yoshida J, Takahashi M. Development of a target-directed magnetic resonance contrast agent using monoclonal antibody-conjugated magnetic p articles. Noshuyo Byori 1996;13:127–32.
[31] Tiefenauer LX, Tschirky A, Kuhne G, Andres RY. In vivo evaluation of magnetite nanoparticles for use as a tumor contrast agent in MRI. Magn Reson Imaging 1996;14:391–402.
[32] Kato M, Neil TK, Fearnley DB, McLellan AD, Vuckovic S, Hart DN. Expression of multilectin receptors and comparative FITC-dextran uptake by human dendritic cells. Int Immunol 2000;12:1511–9.
[33] Gupta AK, Naregalkar RR, Vaidya VD, Gupta M. Recent advances on surface engineering of magnetic iron oxide nanoparticles and their biomedical applications. Nanomed 2007;2:23–39.
[34] Park JW, Hong K, Kirpotin DB, Colbern G, Shalaby R, Baselga J, et al. Anti-HER2 immunoliposomes: enhanced efficacy attributable to targeted delivery. Clin Cancer Res 2002;8:1172–81.
[35] Zhang Y, Kohler N, Zhang M. Surface modification of superparamagnetic magnetite nanoparticles and their intracellul ar uptake. Biomaterials 2002;23:1553–61.
[36] Berry CC, Wells S, Charles S, Curtis AS. Dextran and albumin derivatised iron oxide nanoparticles: influence on fibroblasts in vitro. Biomaterials 2003;24:4551–7.
[37] Panagi Z, Beletsi A, Evangelatos G, Livaniou E, Ithakissios DS, Avgoustakis K. Effect of dose on the biodistribution and pharmacokinetics of PLGA and PLGA-mPEG nanopa rticles. Int J Pharm 2001;221:143–52.
[38] Gabizon AA. Stealth liposomes and tumor targeting: one step further in the quest for the magicbullet. Clin Cancer Res 2001;7:223–5.
[39] Bailon P, Won CY. PEG-modified biopharmaceuticals. Expert Opin Drug Deliv 2009;6:1–16.
[40] Mailander V, Lorenz MR, Holzapfel V, Musyanovych A, Fuchs K, Wiesneth M, et al. Carboxylated superparamagnetic iron oxide particles label cells intracellularly without transfection agents. Mol Imaging Biol 2008;10:138–46.
[41] Weissleder R, Elizondo G, Wittenberg J, Rabito CA, Bengele HH, Josephson L. Ultrasmall superparamagnetic iron oxide: characterization of a new class of contrast agents for MR imaging. Radiology 1990;175:489–93.
[42] Sun C, Sze R, Zhang M. Folic acid-PEG conjugated superparamagnetic nanoparticles for targeted cellular uptake and detection by MRI.J. Biomed Mater Res A 2006;78:550–7.
[43] Matuszewski L, Persigehl T, Wall A, Schwindt W, Tombach B, Fobker M, et al. Cell tagging with clinically approved iron oxides: feasibility and effect of lipofection, particle size, and surface coating on labelling efficiency. Radiology 2005;235:155–61.
[44] Wilhelm C, Gazeau F. Universal cell labelling with anionic magnetic nanoparticles. Biomaterials 2008;29:3161–74.
[45] Cartiera MS, Johnson KM, Rajendran V, Caplan MJ, Saltzman WM. The uptake and intracellular fate of PLGA nanoparticles in epithelial cells. Biomaterials 2009;30:2790–8.
[46] Thorek DL, Chen AK, Czupryna J, Tsourkas A. Superparamagnetic iron oxide nanoparticle probes for molecular imaging. Ann Biomed Eng 2006;34:23–38.
[47] Briley-Saebo K, Bjornerud A, Grant D, Ahlstrom H, Berg T, Kindberg GM. Hepatic cellular distribution and degradation of iron oxide nanoparticles following single intravenous injection in rats: implications for magnetic resonance imaging. Cell Tissue Res 2004;316:315–23.